Microscopic calculation for Ne on NaF at 45 MeV per nucleon

J. Gallego, S. Das Gupta, C. Gale, S. J. Lee,* and C. Pruneau
Physics Department, McGill University, Montréal, Québec, Canada H3A 2T8

S. Gilbert†
Département de Physique, Université Laval, Québec, Québec, Canada G1K 7P4
(Received 11 January 1991)

We present theoretical calculations for data pertaining to Ne on NaF collisions at 45 MeV per nucleon. The calculations use the Boltzmann-Uehling-Uhlenbeck model, modified to incorporate fluctuations. The recent numerical technique developed by Lenk and Pandharipande is applied to test particle propagation in the nuclear mean field. We find that the agreement with experimental data ranges from good to very good.

I. INTRODUCTION

The experimental study of near central collisions of heavy ions at beam energy 30–100 MeV/nucleon is of much current interest. Based on the knowledge acquired so far, one expects to see a transition from a decay predominantly by evaporation to the phenomenon of multifragmentation. Consequently, there is a strong need to use theoretical models to these reactions so as to assess their applicability for describing such phenomena. In this paper we will present theoretical calculations for one such experiment. Details of the experiment are available from other sources.[1,2] Here we will summarize the salient features of this experiment that are needed to understand the theoretical work presented here.

We chose to concentrate on a specific reaction which was ^{20}Ne on NaF at 45 MeV/nucleon, at the National Superconducting Cyclotron Laboratory in Michigan State University (MSU). The experimental setup consisted of two main detectors; a forward charge detector, built at the Chalk River Laboratories, which measured the total charge Z of particles emerging in a forward cone spanning 2.5° to 17°. The energy threshold for particle detection there was 15 MeV/nucleon. The other principal detector was the MSU 4π array. The polar angle coverage for this detector is 19° to 161° with particle detection threshold at 17 MeV/nucleon. The 4π detector was primarily used to tag the multiplicity M (=number of charged particles) on an event-by-event basis. On the basis of similar experiments at higher energies, one might expect an anticorrelation between the readings at the forward detector and the 4π detector. A large total charge at the forward detector could signify a peripheral collision; one would then expect M to be small. By extension, a small number of charges in the forward detector accompanied by a large M value in the 4π detector could be the signal of a central-like collision. Inclusive cross sections of $Z=1$ particles (protons, deuterons, and tritons) integrated over a large angular range as well as over a limited angular range are available. These data are also available as a function of M, the multiplicity in the 4π detector. In the sections to follow we will present these data along with our calculated results. In order to test the validity of the scenarios described above, we have submitted our calculations to the same cuts as the experimental data.

II. THE MICROSCOPIC MODEL

The microscopic model we use is the Boltzmann-Uehling-Uhlenbeck (BUU) model[3] modified so as to enable us to attempt an event-by-event description. This is necessary in order to connect with data. As is well known, the standard BUU model will not produce clusters for equal ion central collisions. This approach solves for the time evolution of the one-body phase-space distribution. Rather than a single event, the BUU model describes an average over many events. The basics of the extended BUU model that we will use here have been described before;[3–6] nonetheless, a few technical yet important points are different for this calculation. We now proceed to explain these details.

There are two inputs to such calculations: the mean field and the hard collisions. We characterize the nuclear mean field by a potential-energy density:

$$v(\mathbf{r})=\frac{A}{2}\rho^2(\mathbf{r})+\frac{B}{\sigma+1}\rho^{\sigma+1}(\mathbf{r}) +\frac{1}{2}\rho(\mathbf{r})\int d^3r' v(\mathbf{r},\mathbf{r}')\rho(\mathbf{r}') , \quad (1)$$

where $v(\mathbf{r},\mathbf{r}')$ is a finite range force and the rest is a Skyrme-type parametrization. Equation (1) implies that the nuclear mean field felt by a nucleon is

$$u(\mathbf{r})=A\rho(\mathbf{r})+B\rho^{\sigma}(\mathbf{r})+\int d^3r' v(\mathbf{r},\mathbf{r}')\rho(\mathbf{r}') . \quad (2)$$

For the finite range force $v(\mathbf{r},\mathbf{r}')$ we use a Yukawa:

$$v(\mathbf{r},\mathbf{r}')=V_0\frac{\exp(-|\mathbf{r}-\mathbf{r}'|/a)}{|\mathbf{r}-\mathbf{r}'|/a} . \quad (3)$$

The parameters of this force are taken from Ref. 7. These are $A=-1563.6$ MeV fm^3, $B=2805.5$ MeV fm$^{7/2}$, $\sigma=\frac{7}{6}$, $V_0=-668.65$ MeV, and $a=0.45979$ fm. With these parameters the binding energy per nu-

cleon in nuclear matter is 15.77 MeV. The value of "a" is the same as used by Bonche, Koonin, and Negele.[8] In addition to the nuclear force, we also include the Coulomb interaction.

The parameters of the mean field, aside from having important effects on the dynamics of heavy-ion collisions, also determine the ground states of colliding nuclei in a self-consistent procedure. Our heavy-ion collision calculations begin with two such ground states approaching each other. These ground states are those obtained in the Thomas-Fermi approximation with the force of Eqs. (1) and (2). The ground-state density of ^{20}Ne in the Thomas-Fermi approximation is shown in Fig. 1. The calculated binding energy per nucleon for ^{20}Ne is 8.48 MeV; for the deuteron and the alpha the corresponding numbers are 4.85 and 6.10 MeV. Note that in the Thomas-Fermi approximation more realistic surfaces for finite nuclei can be obtained with force parameters that give a higher binding energy in nuclear matter (ours give 15.77 MeV) and a higher surface energy in semi-infinite nuclear matter.[9] The numerical recipe used to obtain Thomas-Fermi solutions in finite nuclei is given in Ref. 7.

Given the Thomas-Fermi solution, the phase-space density is mapped by test particles. Usually this needs a Monte Carlo simulation as well as choosing a form factor or else an averaging prescription.[3] Recently, Lenk and Pandharipande[10] have developed a technique for mean-field propagation which gives very accurate conservation of the total energy and the total momentum. This has been incorporated in our own calculation. The available configuration space is partitioned into a lattice of cubic cells of volume $(\delta l)^3$. The density at a lattice site α centered at $\mathbf{r}_\alpha$ is

$$\rho_\alpha \equiv \rho(\mathbf{r}_\alpha) = \sum_i^{N_t A} S(\mathbf{r}_\alpha - \mathbf{r}_i) , \tag{4}$$

where N_t is the number of test nucleons per real nucleon. The form factor $S(\mathbf{r}_\alpha - \mathbf{r}_i)$ must satisfy at all times the constraint

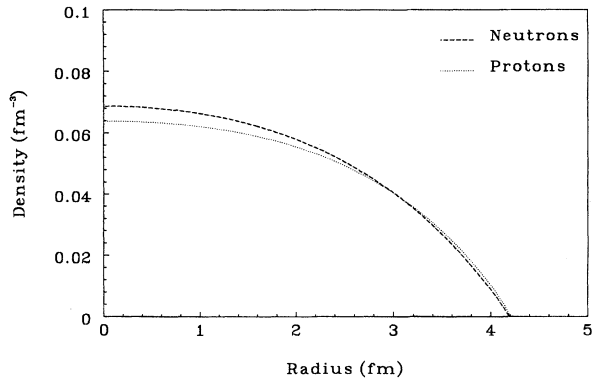

FIG. 1. The density distributions obtained self-consistently in the Thomas-Fermi approximation are shown separately for protons and neutrons, in the case of ground-state ^{20}Ne. The parameters of the interactions are given in the text.

$$(\delta l)^3 \sum_\alpha S(\mathbf{r}_\alpha - \mathbf{r}) = \frac{1}{N_t} , \tag{5}$$

independent of $\mathbf{r}$. Here we use

$$S(\mathbf{r}_\alpha - \mathbf{r}_i) = \frac{1}{N_i b^3} \Theta(1 - |\Delta_{\alpha i}^x|) \Theta(1 - |\Delta_{\alpha i}^y|) \Theta(1 - |\Delta_{\alpha i}^z|) , \tag{6}$$

with $\Delta_{\alpha i}^x = (r_\alpha^x - r_i^x)/b$, setting $N_t = 100$, $(\delta l)^3 = 1$ fm^3, and $b = 1$ fm. Given the lattice density one can then calculate the total interaction energy as a sum over sites of the interaction energy density ϵ_α,

$$V^q = N_t (\delta l)^3 \sum_\alpha \epsilon_\alpha^q , \tag{7}$$

q denoting the isospin of the nucleon species under consideration. The lattice Hamiltonian is written as

$$\mathcal{H} = \sum_i^{N_t A} \frac{p_i^2}{2m} + N_t (\delta l)^3 \sum_\alpha (\epsilon_\alpha^p + \epsilon_\alpha^n) , \tag{8}$$

from which one can derive the equations of motion:

$$\dot{r}_i^{s,q} = \frac{p_i^{s,q}}{m} , \dot{p}_i^{s,q} = -N_t (\delta l)^3 \sum_\alpha \mathcal{U}_\alpha^q \frac{\partial \rho_\alpha}{\partial r_i^{s,q}} = -N_i (\delta l)^3 \sum_\alpha \mathcal{U}_\alpha^q \frac{\partial S(\mathbf{r}_\alpha - \mathbf{r}_i)}{\partial r_i^{s,q}} , \tag{9}$$

$\mathcal{U}_\alpha^q$ being the potential acting on isospin species q. In the calculations discussed in this work, we define

$$\mathcal{U}_\alpha^p = \mathcal{U}_\alpha^1 + \mathcal{U}_\alpha^y + \mathcal{U}_\alpha^c , \tag{10}$$

$$\mathcal{U}_\alpha^n = \mathcal{U}_\alpha^1 + \mathcal{U}_\alpha^y \tag{11}$$

with

$$\mathcal{U}_\alpha^1 = A\rho_\alpha + B\rho_\alpha^\sigma ,$$

$$\mathcal{U}_\alpha^y = V_0 (\delta l)^3 \sum_{\alpha'} \frac{\exp(|\mathbf{r}_\alpha - \mathbf{r}_{\alpha'}|/a)}{|\mathbf{r}_\alpha - \mathbf{r}_{\alpha'}|/a} \rho_{\alpha'} ,$$

$$\mathcal{U}_\alpha^c = e^2 (\delta l)^3 \sum_{\alpha'} \frac{1}{|\mathbf{r}_\alpha - \mathbf{r}_{\alpha'}|} \rho_{\alpha'}^p .$$

Calculating $\mathcal{U}_\alpha^y$ and $\mathcal{U}_\alpha^c$ as written is very time-consuming, and thus we instead solve the associated differential equations

$$\nabla_r^2 \mathcal{U}_\alpha^y - \frac{1}{a^2} \mathcal{U}_\alpha^y = -4\pi a V_0 \rho_\alpha , \quad \nabla_r^2 \mathcal{U}_\alpha^c = -4\pi e^2 \rho_\alpha^r \tag{12}$$

by a relaxation method with Gauss' accelerators.[11,12] Given that the lattice densities are slowly varying functions of time, if one starts with the known potentials at time t, the new solutions at time $t + \delta t$ converge after only 3 iterations of the method.

Inclusion of the finite-range force for the nuclear part allows us to have a more reasonable surface for the self-consistent nuclear ground states of the Thomas-Fermi approximation. Given that in the form factor of Eq. (5), the

width b, for numerical reasons, cannot be taken to the zero, a faithful mapping of density through test particles can only be done if the density does not have a sharp surface, like one would have in the Thomas-Fermi approximation if the nuclear interaction was entirely zero range. We wish to also re-emphasize[13] that the semiclassical model used here suffers from the lack of shell effects; thus the extra binding of the alpha particle is missing in our approximation. Some other approaches to multifragmentation do not suffer from such limitations;[14–16] on the other hand, these approaches do not incorporate dynamics.

We now turn towards hard collisions, the other ingredient in the calculation. We have taken the nucleon-nucleon cross section to be 55 mb and isotropic. The collision cross section between test particles is then σ_{NN}/N_t. We further suppress collisions by a factor $1/N$, but when two test particles collide, $2N_t$ test particles are moved simultaneously. The prescription used is exactly as in Ref. 4. Collisions are thus treated stochastically and are the sources of fluctuation in our model. Recall that N_t is the number of test particles to a physical nucleon.

Other models for fluctuation have been proposed[17] but practical applications to experiments are not available yet. Some model calculations exist which use global fluctuation[18] to get deviation from one time step to another. To study cluster production one in fact needs to create fluctuations which are local in configuration and momentum space. We understand that work towards this goal is in progress.[19]

In calculations like ours one asymptotically observes local pockets of significant density separated from one another against a diffuse background. A composite is obtained when the number of nucleons in a pocket is greater than unity. Thus the number of emerging particles can be found on an event-by-event basis. While this is the general idea, actual answers will somewhat depend upon the precise algorithm used.

The observables we were interested in required that the clusters we produced have an integer number of "real" protons and neutrons. To achieve this we proceeded in two steps. The first of these steps is a coarse-graining sweep where "preliminary clusters" were identified; test nucleons were assigned to a preliminary cluster if their distance to any of the test nucleons already in it was less than a certain value γ in coordinate space. In such an approach, one readily sees that setting γ equal to a very small number is equivalent to scanning for large values of density. In the second step, once all preliminary clusters were identified, the ones whose nucleon number (the number of physical neutrons plus physical protons) was less than 0.5 were rejected, and their constituents temporarily assigned to the background. We then complete the nucleon numbers of the retained clusters as follows: for each cluster, the background test nucleons were arranged according to their phase-space distance to the cluster center of mass. Then as many of the closest background test nucleons as was necessary to get integer proton and neutron numbers were selected. Since a "preliminary cluster" has some neutron and proton content and since the neutron and proton numbers are completed independently, the smallest cluster emerging from a "preliminary cluster" will be $A=2$. All test nucleons still assigned to the background were considered to be free nucleons. We note that the average density of the clusters thus obtained was one third of equilibrium nuclear matter density. Note that the obtained cluster distribution is not a linear function of γ: there is a "critical" value of this parameter beyond which the cluster distribution rapidly saturates to the asymptotic form we compare with experiment. We choose $\gamma=0.225$ fm (this actually corresponds to twice the test nucleon radius if one assumes that the volume it occupies is N_t times smaller than the "real" nucleon volume). Doubling this value changes the number of unbound nucleons by less than 10%.

Fluctuations are automatically included in the one Gaussian per particle approach as used by the Frankfurt group[20] or Boal and associates.[21] Our calculation would have closer resemblance to these models if we used a Gaussian form factor and a single test particle per nucleon.

III. RESULTS

As explained in Sec. II, each simulation in our model corresponds to a single event at an impact parameter of our choice. With the Coulomb and finite-range nuclear forces, following each event up to 200 fm c^{-1} in order to predict clusters requires a computing time of about 16 hours on Vax 750-11. In all, 750 runs were taken, spanning an impact parameter range from 0 to 6 fm. This statistics is adequate for high cross-section events.

Data analysis for this experiment has been done for inclusive spectra of $Z=1$ particles (a) integrated over the whole angular range 19°–161°, (b) integrated over smaller angular ranges, and (c) with specific charge multiplicity in the 4π detector. We compare these results with our calculations. The theoretical differential distributions have been normalized to their experimental counterparts. It should be pointed out that total cross sections have not been a problem in BUU type calculations.

The agreement between experiment and theory is quite reasonable in Fig. 2, where we plot dN/dE, integrated over the whole plastic ball angular coverage. Figure 3 gives more details, separating inclusive distributions into different angular bins. We find when the cross sections are large, theory and experiments agree but there are discrepancies at backward angles where the cross sections are small. Figure 4 presents more exclusive data where inclusive cross sections are shown for fixed multiplicity in the 4π detector; of the cases displayed, $M=5$ represents the most central collisions. We find that the calculations reproduce these very well. For brevity $M=1$ data and calculations are not shown in Fig. 4 although the agreement was just of a similar quality.

An important question at these beam energies is the relationship between charge multiplicity and the impact parameter.[22] Figure 5 shows the results from our calculations. The set of histograms depicts the relative importance in our model of different impact parameter ranges for a given charged-particle multiplicity M. The number

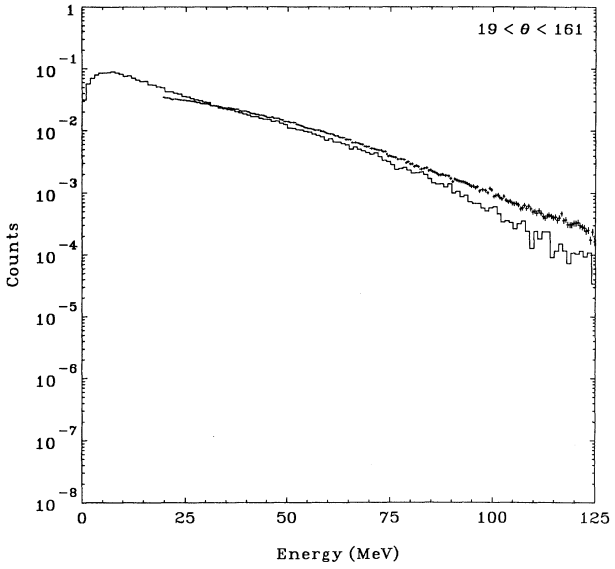

FIG. 2. Inclusive distribution over energy of $Z=1$ particles, integrated over the whole plastic ball polar angle coverage. The data are the solid dots and the calculation is the histogram.

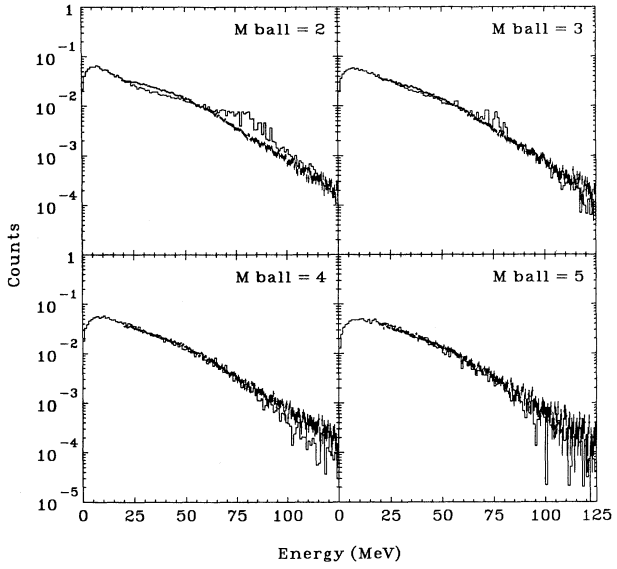

FIG. 4. Inclusive distribution over the energy of $Z=1$ particles, for events contributing to a specific plastic ball multiplicity. The data are the solid dots and the calculation is the histogram.

in parentheses gives the relative probabilities of charge multiplicities in the ball provided the two nuclei hit. While there is no direct comparison of these with experimental data, detailed analyses like this one highlight the impact parameter-multiplicity relationship. Figure 6 shows a plot of ball multiplicity against average charge Z in the forward detector. The error bars on the theoretical points are of a statistical nature. This plot suggests that our connection between multiplicity and the impact parameter may in fact be quite reasonable. The trend of the calculation follows that of the experimental data, with no overlap of the theoretical results with the data in one multiplicity bin only. The anticorrelation discussed in the introduction is in fact observed, both in theory and in

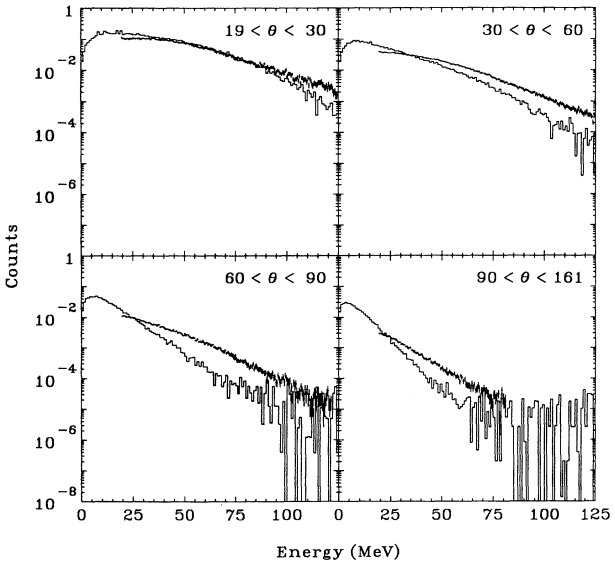

FIG. 3. As in Fig. 2, but for smaller angular ranges.

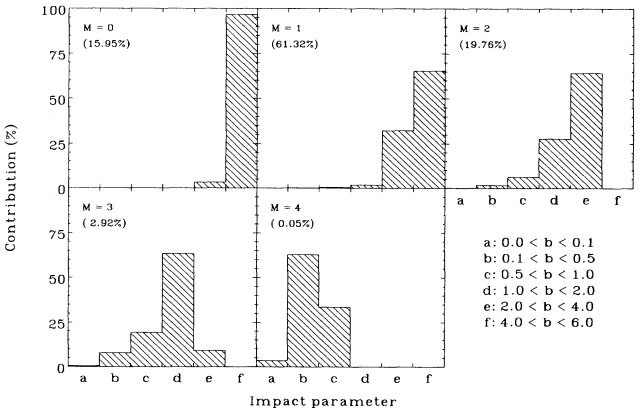

FIG. 5. The individual relative contribution of each impact parameter to a single charged-particle multiplicity in the plastic ball is show. Each histogram corresponds to a fixed multiplicity M. The number in parentheses gives the relative probability of a given charge multiplicity. Note that the maximum impact parameter used in the calculation was $b=6$ fm.

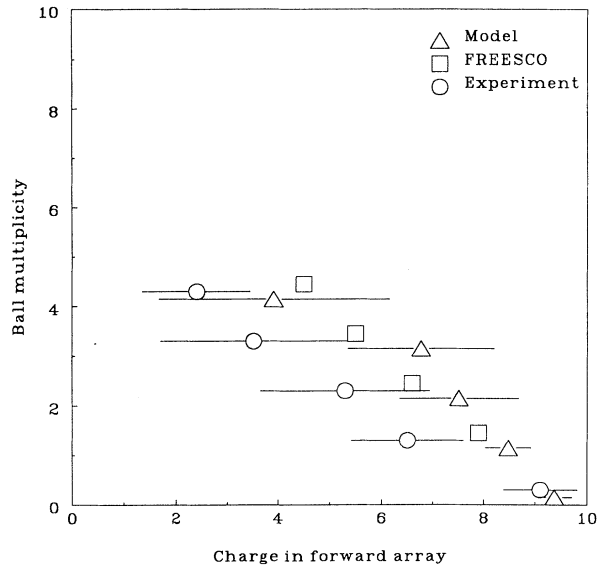

FIG. 6. For a given ball multiplicity, the average total charge in the forward array is shown. For clarity, the different symbols have been slightly offset in the vertical direction. However, they correspond to $M=0,1,2,3,4$ from bottom to top.

experiment. For comparison purposes only, we also show results from FREESCO simulations.[23]

IV. DISCUSSION

This calculation served several purposes. One was to ascertain how well the extended BUU model works in explaining observables in this low-energy range, under more stringent requirements than are usually imposed on calculations of single-particle distributions. The BUU model is not appropriate for describing sequential decay chains. It has a good chance of being successful when sequential decays are a small part of the cross section. Thus the agreement we find in our calculations, especially those displayed in Fig. 4, lends credence to the belief that multifragmentation is an important mode of deexcitation at this energy. Of course, the possibility exists that the particular observables we have calculated do not distinguish between predictions from sequential decays or multifragmentation even though they are different models based on rather different physics. More studies are needed to elucidate this point.

No less important to us was the improvement of the Vlasov propagation that has become possible since the work of Ref. 10. The incorporation of this method has not made it possible to arrive at the results of an extended BUU model with presumably very little contamination from numerical inaccuracies. This point is crucial for calculations done for such low energies, where the associated time scales are longer. The present calculation shows that the results from the model continue to be reasonable. In the future we hope to do more detailed simulations for different systems in the appropriate energy range.

ACKNOWLEDGMENTS

S. Das Gupta, C. Gale, and J. Gallego thank D. Horn and G. Ball for drawing their attention to, and for many discussions about, the experiment. This research is supported in part by the Natural Sciences and Engineering Research Council of Canada and in part by the Québec Department of Education.

*Present address: Physics Dept., Rutgers University, Piscataway, NJ 08855.
†Present address: Physics Dept., McGill University, Montréal, Qué., Canada H3A 2T8.

[1]D. Horn *et al.*, Contribution to the 6th Nordic Meeting on Nuclear Physics, 1989 (Kopervik, Norway, 1989); C. Pruneau *et al.*, AECL report, 1991.
[2]S. Gilbert, MS thesis, Université Laval, 1990.
[3]G. F. Bertsch and S. Das Gupta, Phys. Rep. **160**, 189 (1988).
[4]H. H. Gan, S. J. Lee, and S. Das Gupta, Phys. Rev. C **36**, 2365 (1987).
[5]H. H. Gan and S. J. Lee, Phys. Lett. B **234**, 421 (1990).
[6]W. Bauer, G. F. Bertsch, and S. Das Gupta, Phys. Rev. Lett. **58**, 863 (1987).
[7]S. J. Lee, H. H. Gan, E. D. Cooper, and S. Das Gupta, Phys. Rev. C **40**, 2585 (1989).
[8]P. Bonche, S. E. Koonin, and J. W. Negele, Phys. Rev. C **13**, 1226 (1976).
[9]W. D. Myers, private communication.
[10]R. Lenk and V. Pandharipande, Phys. Rev. C **39**, 2242 (1989).
[11]W. H. Press, B. P. Flannery, S. A. Teukolsky, and W. T. Vetterling, *Numerical Recipes* (Cambridge University Press, Cambridge, England, 1986), pp. 615–667.
[12]S. E. Koonin, K. T. R. Davies, V. Maruhn-Rezwani, H. Feldmeier, S. J. Kreiger, and J. W. Negele, Phys. Rev. C **15**, 1359 (1977).
[13]S. Das Gupta, C. Gale, and J. Gallego, Phys. Rev. C **33**, 1634 (1986).
[14]D. H. E. Gross and H. Massman, Nucl. Phys. **A471**, 339c (1987).
[15]J. Randrup and S. E. Koonin, Nucl. Phys. **A471**, 355c (1987).
[16]J. P. Bondorf, R. Donangelo, H. Schulz, and K. Sneppen, Phys. Lett. **162B**, 30 (1985).
[17]S. Ayik and C. Gregoire, Phys. Lett. B **212**, 269 (1988).
[18]S. Ayik, in Proceedings of the Workshop on Nuclear Dynamics VI, Jackson Hole, Wyoming, 1990, edited by J. Randrup (Report LBL-28709).
[19]S. Suraud, private communication.
[20]J. Aichelin, G. Peilert, A. Bohnet, A. Rosenhauer, H. Stocker, and W. Greiner, Phys. Rev. C **37**, 2451 (1988).
[21]D. H. Boal and J. N. Glosli, Phys. Rev. C **38**, 2621 (1988).
[22]M. B. Tsang, G. F. Bertsch, W. G. Lynch, and M. Tohyama, Phys. Rev. C **40**, 1685 (1989).
[23]G. Fai and J. Randrup, Nucl. Phys. **A404**, 551 (1983).